Journal of Theoretical and Applied Information Technology
15th December 2012. Vol. 46 No.1

ISSN: 1992-8645 www.jatit.org E-ISSN: 1817-3195

ANALOG CIRCUIT INTELLIGENT FAULT DIAGNOSIS BASED ON GREEDY KPCA AND ONE-AGAINST-REST SVM APPROACH

KE GUO, YI ZHU, YE SAN
School of Astronautics, Harbin Institute of Technology, Harbin 150001, Heilongjiang, China

ABSTRACT

Fault diagnosis of analog circuits is essential for guaranteeing the reliability and maintainability of electronic systems. A novel analog circuit fault diagnosis approach based on greedy kernel principal component analysis (KPCA) and one-against-rest support vector machine (OARSVM) is proposed in this paper. In order to obtain a successful fault classifier, eliminating noise and extracting fault features are very important. Due to better performance of nonlinear fault features extraction and noise elimination, KPCA is adopted as a processor. However, a drawback of KPCA is that the storage required for the kernel matrix grows quadratically, and the computational cost for eigenvector of the kernel matrix grows linearly with the number of training samples. Therefore, greedy KPCA which can approximate KPCA with small representation error is introduced to enhance computational efficiency. Based on statistical learning theory and the empirical risk minimization principle, SVM has advantages of better classification accuracy and generalization performance. The extracted fault features are then used as the inputs of OARSVM to solve fault diagnosis problem. The effectiveness of the proposed approach is verified by the experimental results.

Keywords: *Fault Diagnosis, Analog Circuit, Greedy Kernel Principal Component Analysis, One-against-Rest, Support Vector Machine*

1. INTRODUCTION

Analog circuit plays an important role in electronic circuits and systems. Although most part of an electronic system is digital, about 80% of the faults occur in the analog segment [1]. Fault diagnosis in digital electronic circuits has been successfully developed to the point of automation. As compared with the digital circuits, analog circuits fault diagnosis is known to be difficultly due to the huge number of possible faults, the lack of good fault models for analog components similar to the stuck-at-one and stuck-at-zero fault models, which are widely accepted by the digital test community, the presence of components tolerance and the inherent nonlinearity of the circuits. Even linear circuits exhibit nonlinear relations between circuit parameters and the output response.

With the development of electronic technology, the circuit fault diagnosis is also put forward higher requirements. The traditional circuit fault diagnosis approaches such as fault dictionary, *k*-fault hypothesis and network decomposition which need plenty of accessible nodes of the circuit-under-test which have been difficult to adapt to the requirements of modern electronic circuits. In order to solve these problems, automating fault diagnosis using artificial intelligence technique has been a major research topic in the past two decades. Analog circuit fault diagnosis can be regarded as a pattern recognition issue and addressed by machine learning theory. Such as artificial neural networks and support vector machine have been successfully applied to fault diagnosis for analog circuit [2]. In literature [3], the BP neural networks is adopted to the fault diagnosis of linear circuits. Because there is no preprocessing for the impulse response of the circuits, even for relatively small circuits, complex neural networks architecture is demanded for this approach. In literature [4] and [5], the authors have applied BP neural networks with wavelet decomposition and PCA as preprocessors to fault diagnosis of analog circuits. Compared with literature [3], the proposed approach demands a much smaller network and has better diagnostic accuracy. In literature [6], a novel approach for analog fault diagnosis based on BP neural networks and genetic algorithms is proposed nevertheless the approach needs to simultaneously sample the data of several accessible nodes, which is difficult to carry out. That is because only the output node can be accessed directly in the most practical circuits. In literature [2], a novel analog circuit fault diagnosis approach based on improved SVM is proposed, but the drawback of the approach is that the number of

ISSN: 1992-8645 www.jatit.org E-ISSN: 1817-3195

the required accessible nodes is up to 6. In literature [7], a comparison between fuzzy approach and radial basis function networks for soft fault diagnosis in analog circuits is given. The experimental results point out that both approaches provide low classification errors in the presence of noise and non-faulty components tolerance effects.

Support vector machine (SVM) is a relatively new machine learning approach based on the statistical learning theory (SLT) and the empirical risk minimization principle. Compared with the other machine learning methods, such as artificial neural networks, SVM has better generalization and convergence performance [8]. In this paper, SVM is adopted to diagnose fault for analog circuit. In order to obtain a successful SVM-based fault classifier, eliminating noise and extracting fault feature are very important. We know that the fault features of analog circuit that cannot be separated linearly in the input space can be separated linearly in the high dimensional feature space. The output of circuit-under-test (CUT) is sampled in frequency domain and then preprocessed by greedy KPCA to eliminate noise and extract the nonlinear fault features. The fault features are then used as the input of SVM to solve fault diagnosis problem. The paper is organized as follows. In Section 2, kernel principal component and greedy kernel principal component analysis are introduced. In Section 3, a brief overview of SVM and one-against-rest SVM are introduced. Section 4 gives the experimental results and analysis. The conclusions are drawn in the last section.

2. KPCA AND GREEDY KPCA

2.1 KPCA

Principal component analysis (PCA) is a standard linear transformation technique that reduces the number of data dimensions without much loss of data information. Although PCA has been successfully applied in many fields as the most popular dimensionality reduction method, it cannot extract the nonlinear feature in the high dimension data effectively. Kernel principal component analysis (KPCA) successfully extends PCA to nonlinear cases by performing PCA in a higher or even infinite dimensional feature space which is nonlinearly transformed from input space and implicitly defined by a kernel function [9]. The main idea of KPCA is to map the input data $x \in R^m$ into a new high dimensional feature space F firstly via a nonlinear mapping $\phi(\cdot)$, and then perform a linear PCA in F [10].

Let $X = [x_1, x_2, \cdots, x_n]$ ($x_i \in R^m$, $i = 1, 2, \cdots, n$) be the observation set, where n is the sample number, m is the number of variables. By the nonlinear mapping $\phi : x \mapsto \phi(x) \in F^h$, the measured inputs are extended into the high dimensional feature space, where h is the dimension in feature space which is assumed to be a sufficiently large number. The sample covariance matrix in the feature space can be expressed by

$$C_\phi = \frac{1}{n}\sum_{i=1}^{n}(\phi(x_i) - m_\phi)(\phi(x_i) - m_\phi)^T \quad (1)$$

where $m_\phi = \frac{1}{n}\sum_{i=1}^{n}\phi(x_i)$ is the sample mean. We denote $\bar{\phi}(x_i) = \phi(x_i) - m_\phi$ as the centered feature space sample.

Then formula (1) can be expressed as

$$C_\phi = \frac{1}{n}\sum_{i=1}^{n}\bar{\phi}(x_i)\bar{\phi}(x_i)^T \quad (2)$$

For convenience, we assume that $\phi(x_i)$ have been centralized, where $i = 1, 2, \cdots n$.

The kernel principal component can be obtained by solving the eigenvalue problem in the feature space:

$$\lambda v = C_\phi v = \frac{1}{n}\sum_{i=1}^{n}(\bar{\phi}(x_i), v)\bar{\phi}(x_i)^T \quad (3)$$

where eigenvalues $\lambda \geq 0$ and eigenvectors $v \in F$.

It is easy to see that every eigenvector v of C_ϕ lies in the span of $\phi(x_1), \cdots, \phi(x_n)$. Hence $\lambda v = C_\phi v$ is equivalent to

$$\lambda(\phi(x_k), v) = (\phi(x_k), C_\phi v) \quad (4)$$

where $k = 1, 2, \cdots, n$ and there exist coefficients α_i, $i = 1, 2, \cdots, n$

Such that

$$v = \sum_{i=1}^{n}\alpha_i\phi(x_i) \quad (5)$$

Combining equations (4) and (5), we get

$$\lambda\sum_{i=1}^{n}\alpha_i(\phi(x_k), \phi(x_i)) = \frac{1}{n}\sum_{i=1}^{n}\alpha_i(\phi(x_k), \sum_{j=1}^{n}\phi(x_j))(\phi(x_j), \phi(x_i)) \quad (6)$$

ISSN: 1992-8645 www.jatit.org E-ISSN: 1817-3195

Defining kernel matrix K with size $n \times n$ by $[K]_{ij} = (\phi(x_i), \phi(x_j))$, then its elements are determined by virtue of kernel tricks.

$$[K]_{ij} = (\phi(x_i), \phi(x_j)) = \kappa(x_i, x_j) \quad (7)$$

where $\kappa(x_i, x_j)$ is the calculation of the inner product of two vectors in feature space F with a kernel function. This reads

$$n\lambda K\alpha = K^2\alpha \quad (8)$$

where α denotes the column vector with entries $\alpha_1, \alpha_2, \cdots, \alpha_n$. To get solutions of equation (8), we solve the eigenvalue problem, and it is equivalent to perform PCA in F .

$$n\lambda\alpha = K\alpha \quad (9)$$

Let $\lambda_1 \geq \lambda_2 \geq \cdots \geq \lambda_n$ denote the eigenvalues of K , and $\alpha_1, \alpha_2, \cdots, \alpha_n$ the corresponding complete set of eigenvectors. The dimensionality of the problem can be reduced by retaining only the first p eigenvectors. We normalize $\alpha_1, \alpha_2, \cdots, \alpha_p$ by requiring that the corresponding vectors in feature space F be normalized, i.e., $(v_k, v_k) = 1$ for all $k = 1, 2, \cdots, p$.

According to equation (5) we get

$$(\sum_{i=1}^{n} \alpha_i^k \phi(x_i), \sum_{j=1}^{n} \alpha_j^k \phi(x_j)) = 1 \quad (10)$$

Further, we get

$$\begin{aligned}(\sum_{i=1}^{n} \alpha_i^k \phi(x_i), \sum_{j=1}^{n} \alpha_j^k \phi(x_j)) &= \sum_{i=1}^{n} \sum_{j=1}^{n} \alpha_i^k \alpha_j^k K_{ij} \\ &= (\alpha_k, K\alpha_k) \\ &= \lambda_k (\alpha_k, \alpha_k)\end{aligned} \quad (11)$$

Knowing the normalized vectors , the PCs t of a test vector x are then extracted by projecting $\phi(x)$ onto eigenvectors v_k in F , $t_k = (v^k, \phi(x)) = \sum_{i=1}^{n} \alpha_i^k \kappa(x_i, x)$, where $k = 1, 2, \cdots, p$, p is the number of principal components.

In order to avoid performing the nonlinear mappings and computing dot products of the form $(\phi(x), \phi(y))$ in the feature space F , kernel function of form $\kappa(x, y) = (\phi(x), \phi(y))$ is introduced. According to Mercer's theorem which states that any positive semi-definite kernel $\kappa(x, y)$ can be expressed as a dot product in a high-dimensional space. More specifically, if the arguments to the kernel are in a measurable space X, and if the kernel is positive semi-definite, i.e.

$$\sum_{i,j=1}^{n} \alpha_i \alpha_j \kappa(x_i, x_j) \geq 0 \quad (12)$$

for any finite subset $\{x_1, \cdots, x_n\}$ of X and subset $\{\alpha_1, \alpha_2, \cdots, \alpha_n\}$ of real numbers, then there exists a function $\phi(x)$ whose range is in an inner product space of possibly high dimension, such that $\kappa(x, y) = (\phi(x), \phi(y))$.

Mercer's theorem guarantees the existence of a number of kernel functions. Three popular kernel functions are as follows

d^{th} degree polynomial kernel

$$\kappa(x, y) = (x, y)^d \quad (13)$$

Gaussian kernel (Radial basis kernel)

$$\kappa(x, y) = \exp(-\| x - y \|^2 / 2\sigma^2) \quad (14)$$

Sigmoid kernel:

$$\kappa(x, y) = \tanh(c_1(x, y) + c_2) \quad (15)$$

where d , σ , c_1 and c_2 are positive real numbers.

Kernel functions provide a low-dimensional KPCA subspace that represents the distributions of the mapping of the training vectors in the feature space. Before applying KPCA, the centered kernel matrix $\bar{K}$ should be calculated by

$$\bar{K} = K - 1_n K - K 1_n + 1_n K 1_n \quad (16)$$

where $1_n = \frac{1}{n}\begin{bmatrix} 1 & \cdots & 1 \\ \vdots & \ddots & \vdots \\ 1 & \cdots & 1 \end{bmatrix}$.

2.2 Greedy KPCA

Greedy KPCA is proposed by France [11] to reduce training set in feature space F . It is an efficient algorithm to compute the ordinary kernel PCA. The approach aims to represent data in a low dimensional feature space that spanned by the subset of the feature sample set with possibly minimal representation error which is similar to the PCA.

Let $T_F = \{\phi(x_1), \cdots, \phi(x_n)\}$ be a training set of samples represented in the feature space F . Select a subset $S_F \subset T_F$ of the training set such that the

ISSN: 1992-8645 www.jatit.org E-ISSN: 1817-3195

linear span of S_F is similar to the linear span of T_F . Let $I = \{1,2,\cdots,n\}$ denote a set of indices of the training samples T_F and $J = \{j_1, j_2,\cdots, j_l\}$ a set of indices of l selected samples S_F . In such a case $J \subset I$. Let $\tilde{T}_F = \{\tilde{\phi}(x_1),\tilde{\phi}(x_2),\cdots,\tilde{\phi}(x_n)\}$ be an approximation of the training samples T_F represented in the basis given by the selected subset S_F . The approximate feature space representation of the training samples can be expressed as follows:

$$\tilde{\phi}(x_i) = \sum_{j\in J} \beta_{ij}\phi(x_j), \forall i \in I \quad (17)$$

where, the set $J \subset I$ contains indices of l selected samples $S_F = \{\phi(x_j) : j \in J\} \subset T_F$ and $\beta_i \in R^l$ are coefficients of linear combinations.

Assume that the subset S_ϕ is selected from the training set $X_\phi = [\phi(x_1),\cdots,\phi(x_n)]$ and the size of S_ϕ is l . The reconstructed training set $\tilde{X}_\phi = [\tilde{\phi}(x_1), \cdots,\tilde{\phi}(x_n)]$ from subset S_ϕ can be expressed in the compact form

$$\tilde{X}_\phi = S_\phi B \quad (18)$$

where $B = [\beta_1,\cdots,\beta_n]$.

The number l of selected samples J determines the complexity of the $\tilde{\phi}(x_i)$ (in the worst case). The problem of finding the reduced linear span in feature space F can be expressed as an optimization problem. We can take minimum mean square error as the objective function

$$\begin{aligned}&\varepsilon_{MS}(T_F / J) \\ &= \frac{1}{n}\sum_{i\in I} \| \phi(x_i) - \tilde{\phi}(x_i) \|^2 \\ &= \frac{1}{n}\sum_{i\in I} \| \phi(x_i) - \sum_{j\in J} \beta_{ij}\phi(x_j) \|^2\end{aligned} \quad (19)$$

As shown in the literature, the optimal coefficients β_i can be computed as

$$\begin{aligned}\beta_i &= \arg\min_{\beta\in R^l} \left\| \phi(x_i) - \sum_{j\in J} \phi(x_j)[\beta_i]_j \right\|^2 \\ &= (K_S)^{-1}\kappa_S(x_i), \ \forall i \in I\end{aligned} \quad (20)$$

where $K_S \in R^{l\times l}$ is a kernel matrix of the selected sample set S_F and the vector $\kappa_S(x_i) = [\kappa(x_{j1}, x_i), \cdots,\kappa(x_{jl}, x_i)]^T \in R^l$.

The objective function $\varepsilon_{MS}(T_F / J)$ can be rewritten as

$$\begin{aligned}\varepsilon_{MS}(T_F / J) &= \frac{1}{n}\sum_{i\in I}(\kappa(x_i, x_i) - \\ &2K_S\kappa_S(x_i) + (\kappa_S(x_i), K_S\kappa_S(x_i)))\end{aligned} \quad (21)$$

In order to select S_F efficiently, as shown in the literature, firstly, the minimum mean square error can be upper bounded by

$$\begin{aligned}&\varepsilon_{MS}(T_F / J) = \frac{1}{n}\sum_{i\in I} \| \phi(x_i) - \tilde{\phi}(x_i) \|^2 \\ &\le \frac{n-l}{n} \max_{j\in I \setminus J} \| \phi(x_j) - \tilde{\phi}(x_j) \|^2\end{aligned} \quad (22)$$

where $l = Card(J)$ is the number of selected samples in the set J .

Secondly, we can use orthonormalized basis $W = [w_1,\cdots,w_m]$ and the selected subset S_F to evaluate the approximated data and partial reconstruction error efficiently.

$$\tilde{\phi}(x) = W\phi(z) \quad (23)$$

where $\phi(z)$ is a new representation of $\phi(x)$.

The reconstruction error ε_i is computed as

$$\begin{aligned}\varepsilon_i &= \left\| \phi(x_i) - \tilde{\phi}(x_i) \right\| \\ &= (\phi(x_i),\phi(x_i)) - (\phi(z_i),\phi(z_i)), \ \forall i \in I\end{aligned} \quad (24)$$

Finally, the kernel matrix can be computed by using $K \approx Z^T Z$, the reduced kernel matrix K is an $l \times l$ matrix where $l \ll n$.

Then the optimization problem can be solved by the greedy algorithm as shown below.

Greedy minimization of upper bound on $\varepsilon_{MS}(T_F / J)$

1) Initialization. Set $J^{(0)} = \{\varnothing\}$,
$\varepsilon_i^0 = \kappa(x_i, x_i), i \in I$.
2) For $t = 1$ to l
① $j_t = \arg\max_{j\in I\setminus J} \varepsilon_j^{t-1}$
② $[z_i]_t = \frac{1}{\sqrt{\varepsilon_{j_t}^{t-1}}}\left(\kappa(x_i, x_{j_t}) - \sum_{h=1}^{t-1}[z_i]_h[z_{j_t}]_h\right)$, $\forall i \in I$
③ $\alpha_t = \frac{1}{\sqrt{\varepsilon_{j_t}^{t-1}}}\left(\delta(t) - \sum_{i=1}^{t-1}[z_{j_t}]_i\alpha_i\right)$
④ $\varepsilon_i^{(t)} = \varepsilon_i^{(t-1)} - ([z_i]_t)^2, \forall i \in I$
⑤ $J^{(t)} = J^{(t-1)} \cup \{j_t\}$

Obviously, the iteration number of the Greedy KPCA algorithm equals to l . Nonetheless, it is reasonable to terminate the algorithm earlier, if one

ISSN: 1992-8645 www.jatit.org E-ISSN: 1817-3195

of the terminal conditions as shown below is satisfied:

(a) The algorithm halts if the mean square reconstruction error $\varepsilon_{MS}(T_F / J)$ falls below pre-specified limit;

(b) The algorithm halts if $Card(J^{(t)})$ reaches a pre-specified limit;

(c) The algorithm halts if maximum error $\max_{j \in I \setminus J} \| \phi(x_j) - \tilde{\phi}(x_j) \|^2$ falls below pre-specified limit. The use of a particular terminal condition depends on a practical application.

2.3 A Simple Example

In order to show that KPCA has better ability of nonlinear feature extraction and noise elimination, the following system with three variables but only one factor is adopted [12].

$$\begin{aligned} x_1 &= t + e_1 \\ x_2 &= t^2 - 3t + e_2 \\ x_3 &= -t^3 + 3t^2 + e_3 \end{aligned} \tag{25}$$

where e_1, e_2 and e_3 are independent noise variables $N(0, 0.01)$, and $t \in [0.01, 2]$.

Normal data comprising 100 samples were generated according to these equations.

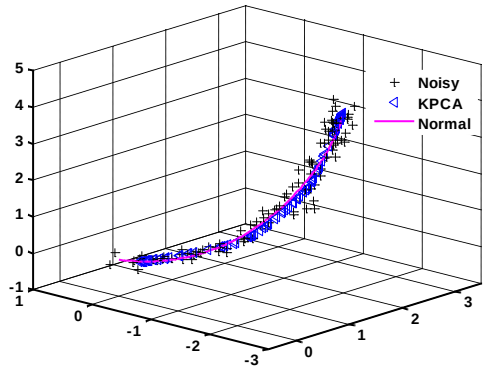

Figure 1: Comparison Between Noisy Data And Reconstructed Data By KPCA

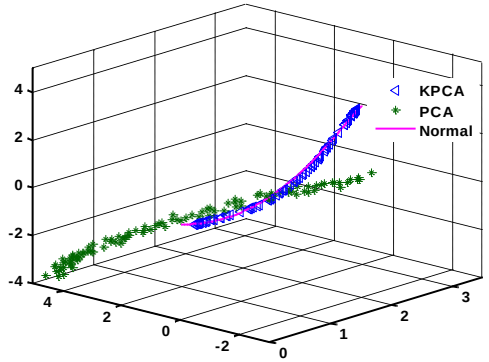

Figure 2: Comparison Between Reconstructed Data By KPCA And PCA

From Figure 1 and Figure 2, it is seen clearly that the nonlinear data have been reconstructed splendidly using KPCA due to better ability of nonlinear feature extraction and noise elimination as compared with PCA.

3. ONE-AGAINST-REST SVM

SVM is originally designed for binary classification. However, the practical issues often require the discrimination for more than two categories, especially in fault diagnosis field. How to extend SVM for multi-class classification issues effectively is still an ongoing research issue. In practice, the multi-class issues can be decomposed into a series of binary classification issues and then solved by binary SVMs.

3.1 Support Vector Machine

Given a training set $T = \{(x_1, y_1), \ldots, (x_l, y_l)\} \in (R^n \times Y)^l$, where l is the number of samples, $i = 1, 2, \cdots, l$. We refer to $x_i \in R^n$ as the ith sample and $y_i \in Y = \{-1, 1\}$ as its label. The classification problem is to find the hyperplane in a high dimensional feature space H, which divides the sample set in H such that all the points with the same label are on the same side of the hyperplane. SVM is to construct a map $\phi(\cdot)$ from the input space R^n to a high dimensional feature space H and to find an optimal hyperplane (w, b) in H such that the separation margin between the positive and negative examples is maximized. Mathematically, the SVM classification amounts to finding a weight vector w and a threshold b satisfying

$$\begin{aligned} &\min \frac{1}{2} w^T w + c \sum_{i=1}^{l} \xi_i \\ &s.t. \begin{cases} y_i [\phi(x_i) + b] \geq 1 - \xi_i \\ \xi_i \geq 0 \end{cases} \end{aligned} \tag{26}$$

where $i = 1, \cdots, l$, $c > 0$ is a regularization parameter for the tradeoff between model complexity and training error, and ξ_i measures the absolute difference between $w\phi(x_i) + b$ and y_i. Figure 3 gives a binary classification SVM graphical illustration. The balls and squares stand for two separable samples, H is the optimal hyperplane, H_1 and H_2 are the convex hull of each class samples respectively.

Journal of Theoretical and Applied Information Technology
15th December 2012. Vol. 46 No.1

ISSN: 1992-8645 www.jatit.org E-ISSN: 1817-3195

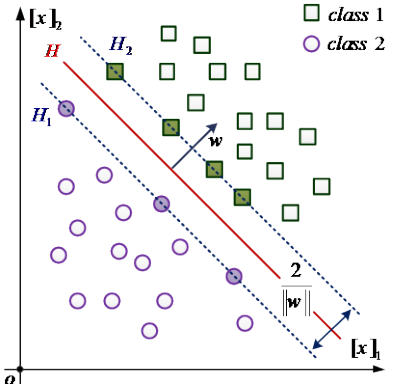

Figure 3: Principle Of Binary Classification SVM

The Lagrange dual format of (27) is easier to solve

$$\min_{\alpha} \frac{1}{2}\sum_{i=1}^{l}\sum_{j=1}^{l} y_i y_j \kappa(x_i, x_j)\alpha_i\alpha_j - \sum_{i=1}^{l}\alpha_i$$
$$s.t. \begin{cases} \sum_{i=1}^{l}\alpha_i y_i = 0 \\ 0 \le \alpha_i \le c \end{cases} \quad (27)$$

where $i = 1, 2, \cdots, l$, $\kappa(x_i, x_j)$ is the kernel function that satisfies $\kappa(x_i, x_j) = \phi(x_i)^T \phi(x_j)$.

Therefore, the learning problem in SVM is equivalent to the convex quadratic programing problem in (26). We have the decision function

$$f(x) = \mathrm{sgn}[g(x)] = \mathrm{sgn}[\sum_{i=1}^{l} y_i\alpha_i\kappa(x_i, x) + b] \quad (28)$$

where $b = y_j - \sum_{i=1}^{l} y_i\alpha_i\kappa(x_i, x_j)$, $\alpha = (\alpha_1, \cdots, \alpha_l)$.

3.2 One-against-rest SVM

In order to solve the multi-class classification problems, we need to extend bin-class SVM for multi-class SVM and there are two mainly used schemes: one-against-rest (OAR) approach and one-against-one (OAO) approach.

In this paper, we adopt the most widely used one-against-rest approach to diagnose the analog circuit. One-against-rest approach constructs *m* sub-classifiers where *m* is the number of classes. The *i*th sub-classifier is trained in the way that all sample points of the *i*th class are labeled with positive and all sample points of other classes labeled with negative. The structure of the OARSVM is shown in Figure 4.

Given a training set $T = \{(x_1, y_1), \ldots, (x_i, y_i)\} \in (R^n \times Y)^l$, where *l* is the number of examples. We refer to $x_i \in R^n$ as the *i*th sample and $y_i \in Y = \{1, 2, \cdots, m\}$ as its label. The *i*th SVM solve the following problem that yields the *i*th decision function $f_i(x) = w_i\phi(x) + b_i$

$$\min_{w,b,\xi} \frac{1}{2}\| w \|^2 + \sum_{i=1}^{l} c_i\xi_i$$
$$s.t. \begin{cases} y_i((w^T\phi(x_i) + b) \ge 1 - \xi_i) \\ \xi_i \ge 0 \end{cases} \quad (29)$$

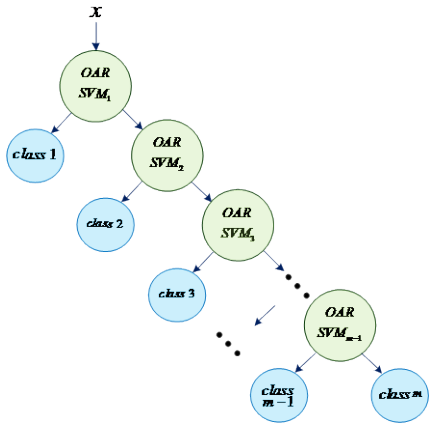

Figure: 4 Structure of OARSVM

At the classification stage, a sample *x* is classified as in class i^* for which f_{i^*} produces the largest value

$$i^* = \arg\max_{i=1,2,\cdots,m} f_i(x) = \arg\max_{i=1,2,\cdots,m}(w_i\phi(x) + b_i) \quad (30)$$

where $b_i = y_j - \sum_{k=1}^{l} y_k\alpha_k^* y_k(\phi(x_k), \phi(x_j))$ and $w_i = \sum_{k=1}^{l}\alpha_k^* y_k\phi(x_k)$.

4. EXPERIMENTAL RESULTS

4.1 Diagnostic Flowchart

The flowchart of analog circuits fault diagnosis based on Greedy KPCA and multi-class SVM is shown in Figure 5, which includes two procedures, namely, the training procedure and the diagnosis procedure. First, we perform 180 Monte Carlo simulations for the fault-free circuit and faulty circuit respectively and the output responses have been randomly divided into two parts including 100 training samples and 80 testing samples. Then, we extract the fault features of the CUT using Greedy KPCA from the training set and construct the one-against-rest SVM.

When performing fault diagnosis, we extract the corresponding major fault features from testing set and import the features to the diagnosis model that

Journal of Theoretical and Applied Information Technology
15th December 2012. Vol. 46 No.1

ISSN: 1992-8645 www.jatit.org E-ISSN: 1817-3195

have been constructed. Then the multi-class SVMs can assort all the fault classes of the CUT.

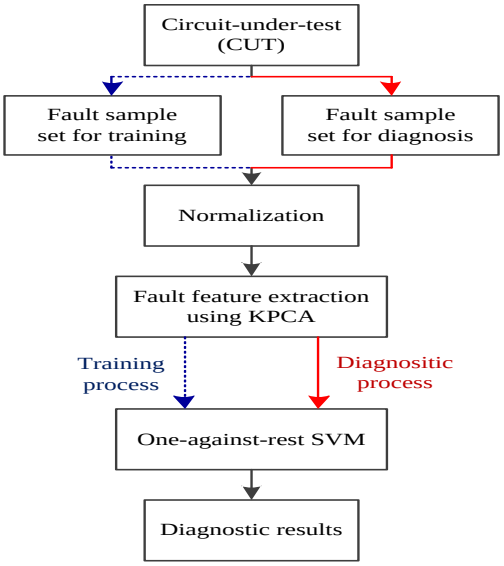

Figure 5: Flowchart Of The Proposed Approach For Analog Circuits Fault Diagnosis

In order to demonstrate the superiority of the proposed approach in feature extraction and fault diagnosis, we compare our approach with PCA-OARSVM approach and OARSVM approach without fault feature extraction and noise elimination, respectively. The number of principal components (PCs) is determined via cumulative percent variance (CPV).

4.2 CUT and Diagnostic Results

Two analog circuits are diagnosed in this section to verify the effectiveness of the proposed approach. The first circuit-under-test (CUT) is Sallen-Key bandpass filter[4], which is a nonlinear circuit. The nominal values of the components which results in a center frequency of 25KHZ are shown in Figure 6. The resistors and capacitors are assumed to have tolerances of 10% and 5%, respectively.

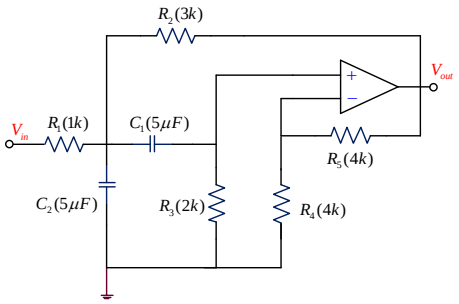

Figure 6: Sallen-Key Bandpass Filter

The frequency response of Sallen-Key filter with the components varying within their tolerances, belong to the fault-free class. The sampled data are preprocessed by greedy KPCA for feature extraction.

In our experiment, four faulty components (C_1, C_2, R_1 and R_3) are chosen by absolute sensitivity analysis, as shown in Figure 7 and Figure 8.

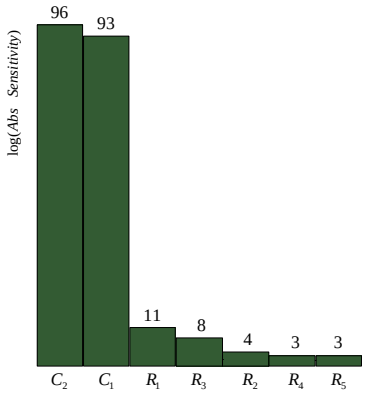

Figure 7: 3db Bandwidth Sensitivity Analysis

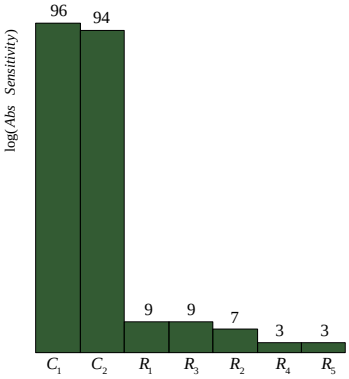

Figure 8: Highpass Cutoff Frequency Sensitivity Analysis

Table 1 : Fault Classes Of Sallen-Key Filter

Fault code	Fault class	Nominal value	Faulty value
F_0	Fault-free	—	—
F_1	$C_1 \uparrow$	5nF	10nF
F_2	$C_1 \downarrow$	5nF	2.5nF
F_3	$C_2 \uparrow$	5nF	10nF
F_4	$C_2 \downarrow$	5nF	2.5nF
F_5	$R_1 \uparrow$	3k Ω	6k Ω
F_6	$R_1 \downarrow$	3k Ω	1.5k Ω
F_7	$R_3 \uparrow$	2k Ω	6k Ω
F_8	$R_3 \downarrow$	2k Ω	1.5k Ω

When any of the four components is higher or lower than its nominal value by 50% with the other three components varying within their tolerances, we obtain the faulty responses. These faulty responses are similarly fed to the greedy KPCA-

Journal of Theoretical and Applied Information Technology
15th December 2012. Vol. 46 No.1

ISSN: 1992-8645 www.jatit.org E-ISSN: 1817-3195

based preprocessors for fault feature extraction so as to form the fault classes $C_1\uparrow$, $C_1\downarrow$, $C_2\uparrow$, $C_2\downarrow$, $R_1\uparrow$, $R_1\downarrow$, $R_3\uparrow$, $R_3\downarrow$, where ↑ and ↓ stand for high and low, respectively. The fault classes and the faulty component values are listed in Table 1.

The 2nd CUT is the four-op-amp biquad highpass filter, which is more complex than the 1st CUT. As shown in Figure 9, the nominal values of the components resulting in a cut-off frequency of 10 kHz. The fault classes and the faulty component values are listed in Table 2, where ↑ and ↓ imply significantly higher or lower than nominal value by 50% similar to the 1st circuit.

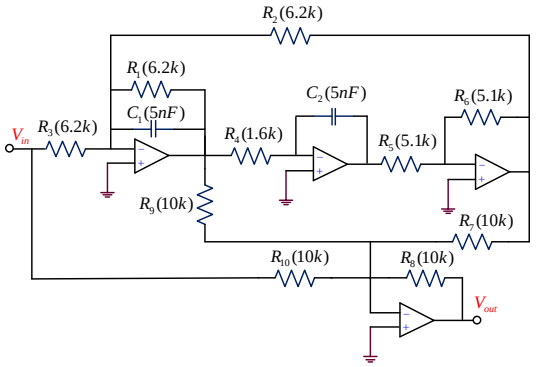

Figure: 9 Four-Op-Amp Biquad Highpass Filter

Table 2: Fault Classes Of Four-Op-Amp Biquad Highpass Filter

Fault code	Fault class	Nominal value	Faulty value
F_0	Fault-free	—	—
F_1	$C_1\uparrow$	5nF	10nF
F_2	$C_1\downarrow$	5nF	2.5nF
F_3	$C_2\uparrow$	5nF	15nF
F_4	$C_2\downarrow$	5nF	1.5nF
F_5	$R_1\uparrow$	6.2k Ω	15k Ω
F_6	$R_1\downarrow$	6.2k Ω	3k Ω
F_7	$R_2\uparrow$	6.2k Ω	18k Ω
F_8	$R_2\downarrow$	6.2k Ω	2k Ω
F_9	$R_3\uparrow$	6.2k Ω	12k Ω
F_{10}	$R_3\downarrow$	6.2k Ω	2.7k Ω
F_{11}	$R_4\uparrow$	1.6k Ω	2.5k Ω
F_{12}	$R_4\downarrow$	1.6k Ω	0.5k Ω

In order to demonstrate the superiority of the proposed approach, the fault features are extracted by PCA and greedy KPCA, respectively. The scatter diagrams of all 9 fault classes of 1st CUT characterized by 2 PCs and 3 PCs using PCA and greedy KPCA approaches are shown in Figure 8 to Figure 12. The contribution rates of the first 5 PCs for PCA and greedy KPCA are given in Table 3. We can see that the CPV of the first 3 PCs for PCA and greedy KPCA are 99.82% and 98.95%, both are more than 95%.

Table 3 : The Contribution Rates Of Pcs For PCA And Greedy KPCA

PC	PCA	Greedy KPCA
PC_1	79.79%	79.08%
PC_2	17.47%	17.39%
PC_3	2.56%	2.48%
PC_4	0.13%	0.78%
PC_5	0.02%	0.17%

The OARSVM are trained by feeding the fault features extracted from the training set. In the experiment, the RBF kernel function $\kappa(x,y) = \exp(-\|x-y\|/2\sigma^2)$ is selected and the kernel width $\sigma = 4$, the penalty parameter $C = 20$. Then we feed the fault features extracted from the test samples into the diagnosis model whose outputs estimate the probabilities that input features belong to different fault classes. The fault diagnosis results of OARSVM without data preprocessing (Approach 1), OARSVM using PCA as a preprocessor (Approach 2) and OARSVM using greedy KPCA as a preprocessor (Approach 3) are listed in Table 4.

Table 4 : Diagnostic Accuracy Of Sallen-Key Filter

Fault code	Diagnostic Accuracy		
	Approach 1	Approach 2	Approach 3
F_0	98.33%	98.33%	100%
F_1	100%	100%	100%
F_2	100%	100%	100%
F_3	100%	100%	100%
F_4	100%	100%	100%
F_5	100%	100%	100%
F_6	100%	100%	100%
F_7	100%	100%	100%
F_8	100%	100%	100%

From Figure 10-14, it is seen clearly that there are only slight overlaps among the fault classes. Approach 2 can obtain nearly the same high diagnostic accuracy, owing to the simple spatial distribution structure of the fault classes.

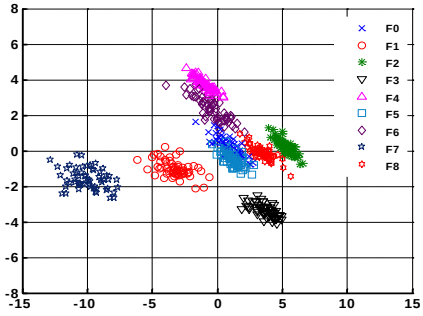

Figure 10: Fault Classes In 2 Dimensional Pca-Based Subspace

Journal of Theoretical and Applied Information Technology
15th December 2012. Vol. 46 No.1

ISSN: 1992-8645 www.jatit.org E-ISSN: 1817-3195

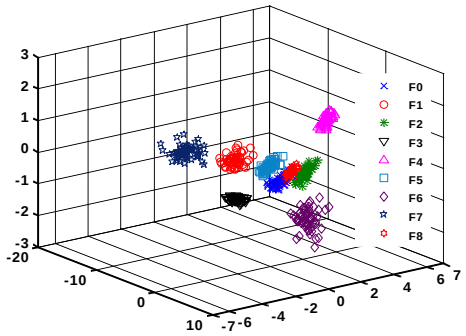

Figure 11: Fault Classes In 3 Dimensional PCA-Based Subspace

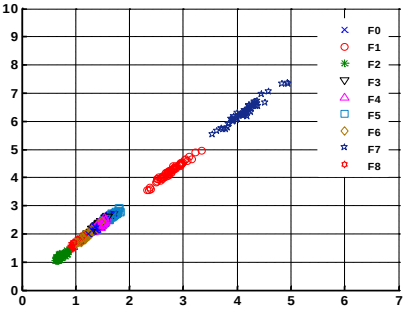

Figure 12: Fault Classes In 3 Dimensional KPCA-Based Subspace

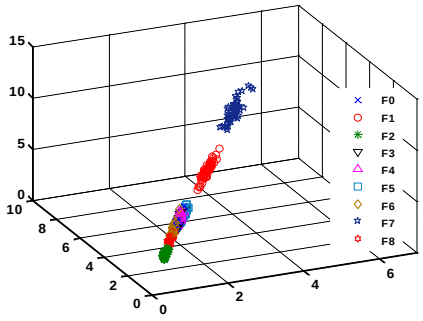

Figure 13: Fault Classes In 3 Dimensional KPCA-Based Subspace

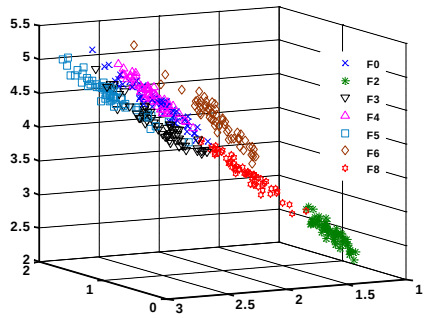

Figure 14: 7 Fault Classes In 3 Dimensional KPCA-Based Subspace

From the diagnostic process of the 2nd CUT, we can see evidently that the proposed approach outperforms approach 1 and approach 2, when the spacial distribution structure of the fault classes is complex. The scatter diagrams of the fault classes for the 2nd CUT in the PCA-based subspace are shown in Figure15 and Figure 16, respectively.

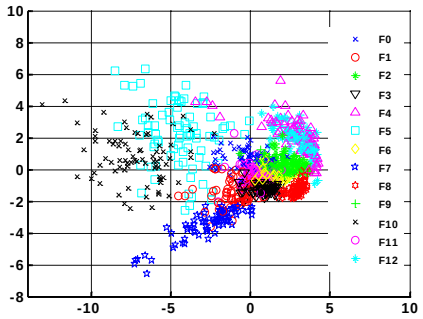

Figure15: Fault Classes In 2 Dimensional PCA-Based Subspace

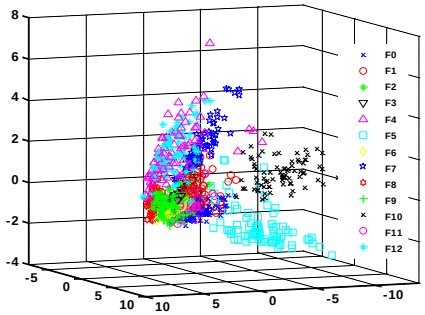

Figure 16: Fault Classes In 3 Dimensional PCA-Based Subspace

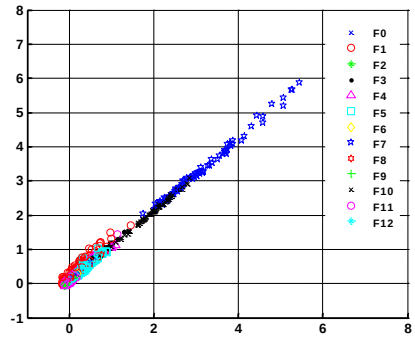

Figure 17: Fault Classes In 2 Dimensional KPCA-Based Subspace

ISSN: 1992-8645 www.jatit.org E-ISSN: 1817-3195

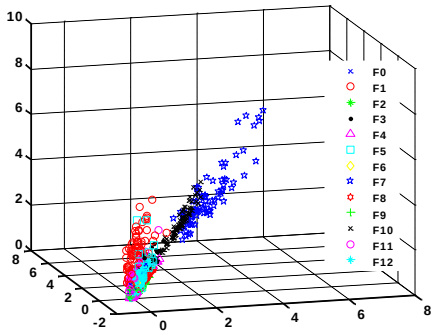

Figure 18: Fault Classes In 3 Dimensional KPCA-Based Subspace

Evidently, there are many overlaps among some fault classes in PCA-based low-dimensional subspace, due to the poor ability of nonlinear fault features extraction. The scatter diagrams of the fault classes in the KPCA-based subspace are shown in Figure 17 and Figure 18, respectively. From these two diagrams, we can see that there are still many overlaps among the fault classes in KPCA-based low-dimensional subspace, but the separabilities of some fault classes are better than which in PCA-based subspace. At most, only the three-dimensional spacial distribution structure of the fault classes can be displayed in form of diagram, which caused the difficulties to exhibit the fact that the separabilities are better in KPCA-based high-dimensional subspace in form of diagram. But this is explained clearly by the contribution rate of each kernel principal component.

From table 5, it is obviously that the 4th PC and the 5th PC can still provide effective nonlinear features information which are useful for fault classification in high-dimensional space compared with the 4th PC and the 5th PC obtained by PCA.

Table 5 : The Contribution Rates Of Pcs For PCA And Greedy KPCA

PC	PCA	Greedy KPCA
PC_1	59.34%	30.90%
PC_2	18.75%	19.62%
PC_3	11.75%	10.76%
PC_4	4.46%	9.71%
PC_5	2.31%	8.38%
PC_6	1.38%	6.86%
PC_7	0.72%	2.89%
PC_8	0.49%	2.28%

The diagnostic results of the 2nd CUT are listed in Table 6. It can be seen that the diagnostic accuracy obtained by the proposed method is higher than the other two approaches on any fault class. After simple calculation, we can get that the average diagnostic accuracy of Approach 1 is 63.77% and Approach 2 is 74.75%, while the average diagnostic accuracy of Approach 3 is 88.73%, when KPCA is used as preprocessor for features extraction. Apparently, the proposed approach obtains the highest average diagnostic accuracy.

Table 6 : Diagnostic Accuracy Of Four-Op-Amp Biquad Highpass Filter

Fault code	Diagnostic Accuracy		
	Approach 1	Approach 2	Approach 3
F_0	12.50%	72.50%	83.75%
F_1	77.50%	87.50%	92.25%
F_2	68.75%	66.25%	90.75%
F_3	68.75%	85.50%	90.00%
F_4	81.25%	81.25%	85.25%
F_5	77.50%	88.75%	93.75%
F_6	27.50%	35.00%	91.25%
F_7	98.75%	100%	100%
F_8	85.00%	91.25%	100%
F_9	55.00%	61.25%	83.75%
F_{10}	95.00%	97.50%	98.75%
F_{11}	26.25%	46.25%	76.25%
F_{12}	55.25%	58.75%	67.75%

5. CONCLUSION

Fault diagnosis of analog circuit is of essential importance for guaranteeing the reliability and maintainability of electronic systems. We have applied OARSVM approach with greedy kernel principal component analysis as preprocessor to diagnose analog circuits. Our work indicates that the proposed preprocessing techniques have a significant impact on analog circuits fault diagnosis, due to the better ability of nonlinear features extraction compared with PCA. Two examples demonstrated that the proposed approach can obtain a high diagnostic accuracy, if the spatial distribution structure of the fault classes is not complex. Even though the separabilites of the fault classes are not high in low-dimensional space, we can make use of the high-dimensional information extracted by greedy KPCA to obtain a satisfactory diagnostic accuracy.

ACKNOWLEDGEMENTS

This work was supported by NSFC (61074127).

REFERENCES:

[1] F Li, Y P Woo, "Fault detection for linear analog IC—The method of short-circuit admittance parameters", *IEEE Transactions on Circuits and Systems I: Fundamental Theory*

ISSN: 1992-8645 www.jatit.org E-ISSN: 1817-3195

and Applications, Vol. 41, No. 9, 2002, pp. 105-108.

[2] C Jiang, Y R Wang, "A novel approach of analog circuit fault diagnosis using support vector machines classifier", *Measurement*, Vol. 44, No. 1, 2011, pp. 281-289.

[3] R Spina, S Upadhyaya, "Linear circuit fault diagnosis using neuromorphic analyzers", *IEEE Transactions on Circuits and Systems II: Analog and Digital Signal Processing*, Vol. 4, No. 3, 1997, pp. 188-196.

[4] M Aminian, F Aminian, "Neural network based analog circuit fault diagnosis using wavelet transform as preprocessor", *IEEE Transactions on Circuits and Systems II: Analog and Digital Signal Processing*, Vol. 47, No. 2, 2000, pp. 151-156.

[5] M Aminian, F Aminian, "Neural-Network based analog circuit fault diagnosis using wavelet transform as preprocessor", *IEEE Transactions on Instrumentation and Measurement*, Vol. 51, No. 3, 2002, pp. 544-550.

[6] Y H Tan, Y G He, C Chun, "A novel method for analog fault diagnosis based on neural networks and genetic algorithms", *IEEE Transactions on Instrumentation and Measurement*, Vol. 51, No. 11, 2008, pp. 2631-2639.

[7] C Marcantonio, F Ada, "Soft fault detection and isolation in analog circuits: some results and a comparison between a fuzzy approach and RBF NN", *IEEE Transactions on Instrumentation and Measurement*, Vol. 51, No. 1, 2002, pp. 196-202.

[8] R Moraes, J F Valiati, N Gavião, "Document-level sentiment classification: An empirical comparison between SVM and ANN", *Expert Systems with Applications*, Vol. 40, No. 2, 2013, pp. 621-633.

[9] B Schölkopf, A Smola, "Nonlinear component analysis as a kernel eigenvalue problem", *Neural Computation*, Vol. 10, No. 6, 1998, pp. 1299-1319.

[10] M B Richman, I Adrianto, "Classification and regionalization through kernel principal component analysis", *Physics and Chemistry of the Earth*, Vol. 35, No. 9, 2010, pp. 316-328.

[11] V Franc, V Hlavác, "Greedy kernel principal component analysis", *Lecture Notes in Computer Science*, Vol. 3948, No. 1, 2006, pp. 87-105.

[12] D Dong, T J Mcavoy, "Nonlinear Principal Component Analysis—Based on Principal Curves and Neural Networks", *Computers and Chemical Engineering*, Vol. 25, No. 1, 1996, pp. 65-78.